Research Article Vol. 29, No. 16 / 2 August 2021 / Optics Express 24989

Optics EXPRESS

Light trapping transparent electrodes with a wide-angle response

MENGDI SUN[1] AND PIETER G. KIK[1,2,*]

[1] CREOL, The College of Optics and Photonics, University of Central Florida, Orlando, Florida 32816, USA
[2] Physics Department, University of Central Florida, Orlando, Florida 32816, USA
[*] kik@creol.ucf.edu

Abstract: The angle dependent transmission of light trapping transparent electrodes is investigated. The electrodes consist of triangular metallic wire arrays embedded in a dielectric cover layer. Normal incidence illumination of the structure produces light trapping via total internal reflection, virtually eliminating all shadowing losses. It is found that varying the external angle of incidence can affect the light trapping efficiency η_{LT} due to partial loss of internal reflection and increased interaction with neighboring wires. Despite these effects, a judicious selection of geometry and materials can reduce shadowing losses by more than 85% over a surprisingly large angular range of 120°. It is demonstrated that the angle-averaged shadowing losses in an encapsulated silicon solar cell under illumination with unpolarized light can be reduced by more than a factor of two for incident angles between −60° and +60° off-normal across the entire AM1.5 solar spectrum.

1. Introduction

Metallic front contacts are widely employed in optoelectronic devices such as photovoltaic devices and high-speed photodetectors [1–13]. The major loss mechanisms in these devices are shading losses, parasitic absorption, resistive losses and recombination losses [14]. The trade-off between optical and electrical performance poses a key challenge to achieving high optical to electrical power conversion efficiency [15,16]. For example, dense metallic front contacts on solar cells reduce resistive losses, but adversely affect optical transmission. On the other hand, a sparse array of thin metallic wires necessitates long charge carrier collection paths which causes strong recombination losses in materials such as silicon [17–22]. To address these challenges, various designs have been studied, including encapsulated front contacts [20,23–25], nanostructures with graded refractive index [26–29] and electrodes that incorporate resonators to enhance absorption [11,30,31]. For instance, Kuang et al. reported a type of encapsulated transparent electrodes with 60%−80% optical transmission at 300–1400 nm wavelength range at incident angles below 60° [20]. Another type of high aspect ratio effective transparent contacts (ETC) without the top cover layer has been reported by Saive et al. [13,32], showing near 100% transmission in the visible regime at normal incidence. Meyer Burger's Multiwire technology also showed the ability of light trapping [33]. For all these approaches, a large transmission (T>~90%) [34,35] over a wide angular response is desirable to enable efficient photovoltaic efficiency for different positions of the sun, or to enable efficient signal collection with high numerical aperture optics.

A new design for achieving transparent electrodes has been introduced that makes use of light trapping to mitigate shadowing losses [36]. In this design metallic front grid lines with a non-coplanar surface are embedded in a dielectric cover layer. Light normally incident on the inclined surfaces is reflected upward at an off-normal angle. When the upward angle is larger than the critical angle (θ_c) of the cover layer, the incident light is trapped via total internal reflection (TIR), almost entirely eliminating shadowing losses. The optical and electronic performance of such structures has been studied as a function of wire size and shape for normal

#431530
Journal © 2021

https://doi.org/10.1364/OE.431530
Received 18 May 2021; revised 1 Jul 2021; accepted 2 Jul 2021; published 21 Jul 2021

incidence illumination [37], showing great potential for use as transparent electrodes. Unlike traditional metallic electrodes where shadowing losses scale linearly with metal coverage, the normal-incidence transmission of light trapping electrodes can remain close to 100% for a metal areal coverage well over 50% [36,37], allowing the realization of transparent electrodes with extremely high electrical conductivity.

An as yet unexplored aspect is the angular response of such light trapping electrodes. In this study we investigate the influence of electrode geometry on the angular response of the transmission, using both analytical and numerical models. It is found that a light trapping efficiency exceeding 85% can be achieved over a 120° angular range, showing the significant promise of this light trapping design for use in photovoltaics and optical detectors that require wide viewing angles and high power conversion efficiency.

2. Light trapping electrode geometry

Figure 1(a) shows a schematic of the interdigitated light trapping electrode structure under consideration. It consists of a periodic array of triangular metallic grid lines embedded in a dielectric cover layer. In real-world PV modules, metal wire electrodes are embedded in an EVA cover layer, which is approximately index-matched with an additional glass cover layer. Light reflected upward into the EVA layer transmits into the glass cover layer with high efficiency. While in this device geometry the surface reflection would occur at larger distance from the electrodes, light reflected at large angle would still undergo TIR at the glass-air interface. To simplify the model, here the cover layer index above and the electrodes is assumed uniform. An anti-reflection coating (ARC) is present on the cover layer. The metal grid lines are taken to be silver [38].

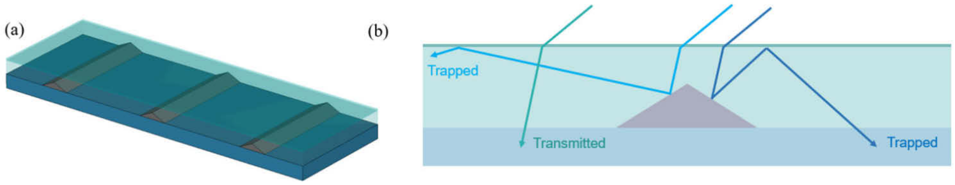

Fig. 1. (a) Schematic of the metallic light trapping electrodes and (b) cross section of single grid line including three example ray paths for off-normal illumination.

Figure 1(b) shows the principle of operation of the triangular light trapping electrode under off-normal illumination. Light entering the cover layer refracts toward the surface normal and either transmits through the electrode gap (cyan arrow) or is reflected upward by the metal line at a modified internal angle (blue arrows). If the upward angle is larger than the critical angle θ_c of the cover layer, the rays subsequently undergo lossless total internal reflection (TIR), redirecting the light into the substrate.

Based on Fig. 1(b) it is clear that varying the external angle of incidence will affect the ray path, which could impact the efficiency of the light trapping process. To study the applicability of this light trapping geometry for use over a wide angular range, the angular response of the electrode transmission will be studied as a function of three electrode parameters: the cover layer thickness, the cover layer index, and the electrode surface tilt angle. The transmission and internal field distributions are investigated using CST Studio [39] and rigorous coupled wave analysis (RCWA) [40], and the results are interpreted using a ray optics model.

3. Influence of cover layer thickness

We first investigate the angle-dependent transmission of an interdigitated light trapping electrode as a function of the cover layer thickness D for a metal coverage of f=25%, with a cover layer index of n_c=2.5, an electrode surface tilt angle of α_s=20°, and a metal grid line width of W=2 µm. The incident wavelength is initially chosen to be 600 nm to represent a typical visible wavelength, and the chosen ARC thickness of d_{ARC}=95 nm and index n_{ARC}=1.58 represent the optimal normal-incidence values for this wavelength. The substrate is initially assumed to be index-matched to the cover layer to facilitate analysis. A similar analysis with a non-index matched substrate and broadband illumination is presented in the final section.

Figure 2(a) shows the transmission of unpolarized 600 nm light determined using RCWA as a function of external angle of incidence θ for cover layer thickness values *D* of 1.6 µm, 2.2 µm, and 4.4 µm, where *D* is the distance from the base of the grid line to the bottom of the ARC layer. Note that two of the curves show transmission values as high as 98% for near-normal incidence illumination, despite the fact that the sample has only 75% open area. This demonstrates near complete recovery of shadowing losses through light trapping.

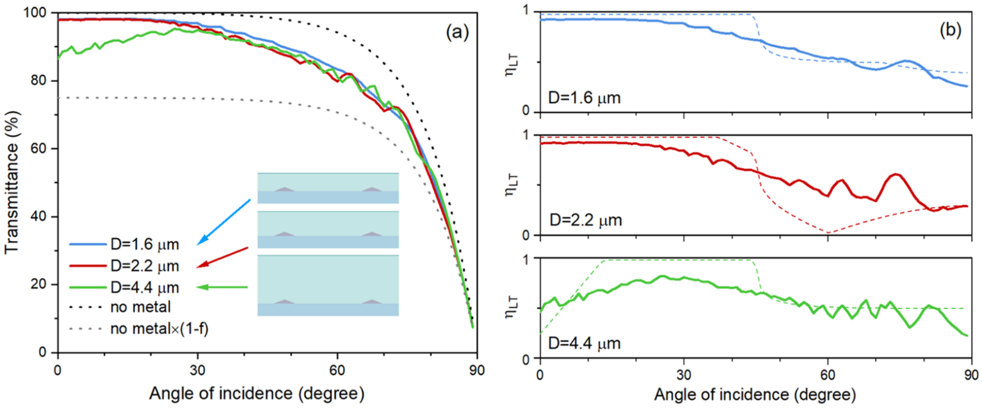

Fig. 2. (a) Transmittance at λ_0=600 nm of light trapping electrodes with 25% metal coverage, W=2 µm, α_s=20°, n_c=2.5 three cover layer thickness values *D*=1.6 µm (blue), 2.2 µm (red) and 4.4 µm (green). (b) Corresponding light trapping efficiencies from numerical calculations (solid lines) and ray optics (dashed lines).

All three curves show a gradual drop in transmission as the external angle of incidence is increased. For comparison, the black dotted line shows the analytically calculated transmission of unpolarized light through the same structure in the absence of metallic lines. This curve, which we will call $T_{max}(\theta)$ sets an upper limit to the transmission, accounting for reduced transmission at high angle due to increased top surface reflection loss. The gray dotted line shows the related quantity $T_{min}(\theta)=(1-f)\cdot T_{max}(\theta)$, which represents the expected transmission in the absence of any light trapping. For cover layer thickness values of 1.6 µm and 2.2 µm the low-angle transmission lies remarkably close to the upper limit of the transmission, indicating very efficient light trapping. As the incident angle is increased, the transmission curves deviate from the calculated upper limit, but stay well above the expected transmission in the absence of light trapping.

To analyze the optical performance of the transparent electrode we introduce the light trapping efficiency η_{LT}, defined as $\eta_{LT}=(T-T_{min})/(T_{max}-T_{min})$. The denominator which is equal to $f\cdot T_{max}$ represents the fraction of light incident on metal that may be recovered via light trapping, while the numerator represents the actual fraction of light that was recovered. Defined this way, η_{LT} is equivalent to the reduction in shadowing losses. The corresponding light trapping efficiencies for the three geometries from Fig. 2(a) are shown in Fig. 2(b) (solid lines). For electrodes with *D*=1.6 µm and 2.2 µm, the light trapping efficiency is close to 100% at small angles, indicating that a large fraction of light incident on the metal is reflected upward at angles larger than the critical angle followed by total internal reflection and transmission into the substrate. As the external angle of incidence is increased, the light trapping efficiency drops gradually, reaching a value of ~25% at glancing angle illumination (θ=90°). In contrast, the electrode with D=4.4 µm shows a relatively low light trapping efficiency of ~50% at normal incidence that briefly rises to ~75% followed by a gradual drop towards higher angles.

To understand the trends observed in Fig. 2(b) a simplified ray optics model was developed where any ray that encounters a metal surface twice is considered lost. Reflection losses at the metal surfaces and partial internal reflection at the top surface are taken into account. The corresponding predicted transmission results are included in Fig. 2(b) as dashed lines. For all three cases the ray optics model predicts a relatively sudden drop in the light trapping efficiency at $\theta = 44°$. This can be understood by considering the critical angle of the cover layer. As the external angle of incidence is increased to positive angles (to the right side of the surface normal), the internal refracted angle increases correspondingly according to Snell's law. This in turn *increases* the angle of the upward ray generated by the left half of the grid line (light blue ray Fig. 1(b)) while *decreasing* the angle of the upward ray generated by the right half of the line (dark blue ray in Fig. 1(b)). As the incident angle reaches $\theta = 44°$ the angle of the latter ray drops below the critical angle of the cover layer, causing a loss of TIR and precluding efficient light trapping. A very subtle additional efficiency drop is seen to start at $\theta = 72°$, which corresponds to the angle at which the left ray impinges on a neighboring grid line, a loss process which we will call secondary shadowing. At a larger cover layer thickness (D=2.2 µm) the same internally reflected ray travels further before reaching the substrate, and consequently secondary shadowing occurs at a smaller angle of incidence of 38°. At D=4.4 µm, secondary shadowing is already present under normal incidence illumination, leading to the relatively low light trapping at small angles.

Comparing the numerical results with the ray optics results in Fig. 2(b) it is evident that the numerically predicted loss of light trapping occurs over a broader angular range than expected from ray optics. This is attributed to diffractive effects: the upward reflected light is generated by a relatively narrow grid line, which introduces significant angular spread in the reflected beam [37]. A second key difference is the near-absence of any evidence of secondary shadowing in the numerical data, which is also attributed to diffractive effects. The angular spread of the reflected

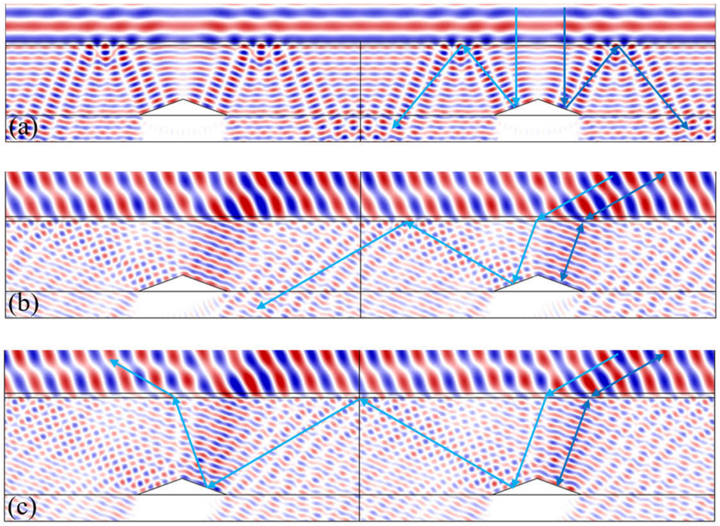

Fig. 3. TE field distributions of 2 µm wide light trapping electrodes in n_c=2.5 at 25% metal coverage with surface tilt α_s=20° for (a) θ=0° and D=1.6 µm, (b) θ=60° and D=1.6 µm and (c) θ=60° and D=2.2 µm.

beams results in a distance dependent width of the reflected beam that increasingly exceeds the adjacent wire width at larger propagation distance. Consequently, only a small fraction of the internally reflected light interacts with an adjacent wire at any given angle of incidence.

Figure 3 shows numerically simulated TE (s-polarized) field distributions around silver light trapping electrodes under 600nm illumination, corresponding to key scenarios discussed above. The wave propagation direction is indicated by the arrows. Figure 3(a) shows the case of near-complete light trapping under normal incidence illumination. Note that while a shadow is present under the wire as evidenced by a lack of wavefronts, there is very little loss of transmission due to the fact that this missing light is recovered by TIR. Figure 3(b) demonstrates that at large external angle of incidence, part of the light incident on the metal grid line is reflected upward at relatively small internal angle. This is indirectly visible as the standing wave pattern above the right half of the grid lines. The reflected light travels upward at an angle below the critical angle, resulting in large transmission back into air, reducing the overall transmission (dark blue arrows). Figure 3(c) shows the field distribution for the same angle of incidence as in Fig. 3(b) but with a larger cover layer thickness of D=2.2 µm, which can introduce secondary shadowing due to an additional radiative loss pathway (light blue arrows).

4. Influence of cover layer index

The preceding section demonstrated that the light trapping efficiency drops significantly when light is reflected at upward angles below the critical angle, causing a loss of TIR. Since the internal angle is affected by the refractive index of the cover layer, the angular performance of light trapping electrodes is expected to depend critically on the refractive index of the cover layer. To evaluate this aspect, we investigate the angular response of the electrodes for three values of the cover layer index: n_c=1.5 representative of glass (θ_c=41.8°), n_c=2.2 representative of e.g. aluminum nitride (θ_c=27°) and n_c=4 representative of e.g. silicon (θ_c=14.5°). The geometry is kept fixed with f=0.25, α_s=15°, W=2 µm, and D=1 µm as shown in the inset of Fig. 4(a). The small cover layer thickness was chosen to minimize the risk of secondary shadowing.

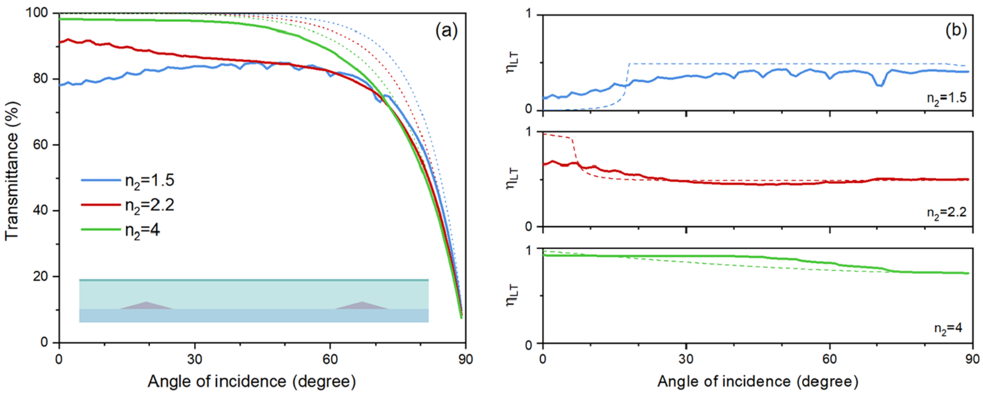

Fig. 4. (a) Transmittance of light trapping electrodes with f=0.25, W=2 µm, D=1 µm, α_s=15° for three different cover index values n_c=1.5 (blue), 2.2 (red) and 4 (black). The dotted lines represent transmission in the absence of metal. (b) Corresponding light trapping efficiencies from numerical calculations (solid lines) and ray optics (dashed lines).

Figure 4(a) shows the calculated angle-dependent transmission for the three choices of cover layer index. Similar to the observations in Fig. 2, all transmission curves drop steeply at high angle of incidence which is predominantly due to top surface reflection losses. This is confirmed by the $T_{max}(\theta)$ curves, representing the same structures without metal (dotted lines). Note that all curves show a small-angle transmission larger than 75% with f=0.25, indicating that some degree of light trapping is achieved in all three cases. For incident angles below 45° the higher index cover layers are seen to yield larger optical transmission.

Figure 4(b) shows the corresponding light trapping efficiency curves (solid lines) from numerical calculations and based on the previously discussed ray optics model (dashed lines). For a cover layer index of n_c=1.5 (blue line) the numerically determined light trapping efficiency at normal incidence is low (∼12.8%), and near-zero according to the ray optics model. This is due to the fact that TIR is not achieved for these parameter choices. Under normal incidence illumination, the upward rays appear at an angle of 30° (twice the surface tilt, independent of refractive index) which is below the critical angle of 42° at this index, resulting in transmission of the reflected rays back into air. This case is illustrated for TE illumination in Fig. 5(a). Note the significant lateral variation of the electric field strength outside the electrode structure, indicative of interference of the incident plane wave and high-angle light exiting the structure. As the angle of incidence is increased, the angle of the left upward ray increases, leading to the onset of light recovery through TIR at an incident angle of 18°. TIR is not achieved for the right ray at any positive external angle. An example field distribution for this scenario is shown in Fig. 5(b) for θ=30°. The lack of TIR for light incident on the right side of the grid line results in the observed upper limit of 50% light trapping efficiency in the top panel of Fig. 4(b).

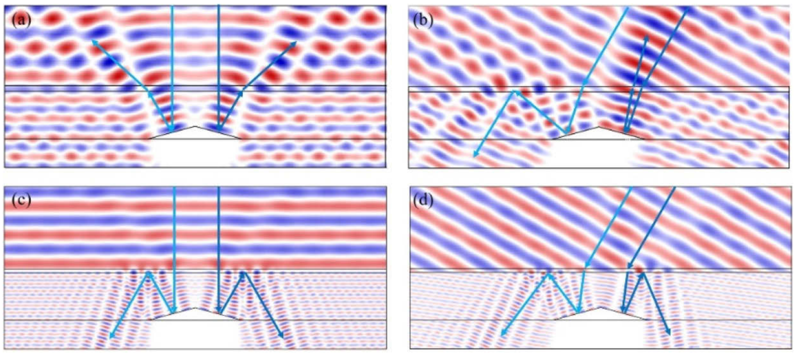

Fig. 5. TE field distributions of light trapping electrodes with f=0.25, W=2 µm, α_s=15°, D=1 µm for a cover layer index of n_c=1.5 at (a) normal incidence and at (b) 30° angle of incidence, and for a cover layer index of n_c=4 at (c) normal incidence and (d) 30° angle of incidence.

For intermediate cover layer index (n_c=2.2) the normal incidence light trapping efficiency starts at ∼65.5% and drops gradually to ∼50% as the incident angle is increased. The ray optics model clarifies these observations: at normal incidence, the reflected rays again appear at 30° which in this case is above the critical angle of θ_c=27° for this refractive index. While this in principle this would allow for efficient light trapping, the angular spread of the reflected beam due to the previously discussed diffractive effects leads to significant radiative losses. As the incident angle is increased beyond θ=12°, TIR is lost for the right upward ray, resulting in a lower light trapping efficiency of ∼50%.

Remarkably, when using a large cover layer index (n_c=4) the simulated light trapping efficiency exceeds 73% for all incident angles and is above 85% over a 120° angular range. This large suppression of shadowing loss over such a wide angular range is the result of two related effects. First, the high index causes strong refraction as the light enters the cover layer, and consequently the light is incident on the grid line at near-normal incidence even for large external angles. Second, due to the small critical angle of θ_c=14.5°, light trapping is achieved even at small internal angles. Figure 5(c) shows the corresponding TE field distribution for normal incidence illumination. Note the absence of lateral variation of the external wavefronts, indicative of efficient light trapping. Figure 5(d) shows the same structure for 30° angle of incidence. Note that even though the incident angle increased significantly, the changes in the internal ray paths compared to Fig. 5(c) are relatively small due to the strong refraction, and thus trapping remains efficient. The external wavefronts remain approximately planar even at this large angle of incidence, indicative of small surface reflection and efficient light trapping.

5. Influence of surface tilt angle

In the preceding section, it was observed that normal incidence illumination for n_c=1.5 and α_s=15° TIR was not achieved, resulting in low light-trapping efficiency. This problem can be mitigated by using larger surface tilt. In the following we evaluate the light trapping performance for three surface tilt angles: α_s=0°, 15°, and 30°. The remaining parameters are held fixed at f=0.25, n_c=1.5, W=2 µm, and D=1 µm.

Figure 6(a) shows the simulated angle-dependent transmittance for all three choices of surface angle. As before, the loss of transmission at high angle is largely due to top-surface reflection, and all curves lie almost entirely between the estimated maximum (perfect light trapping, black dotted line) and minimum transmittance (zero light trapping, gray dotted line) curves. Figure 6(b) shows the corresponding light trapping efficiency curves, as well as the predicted light trapping efficiency based on ray tracing. The top panel shows the results for flat embedded electrodes, similar to standard flat top electrodes on silicon solar cells. As expected, flat electrodes exhibit near zero trapping efficiency at small angles. A distribution of the TE field magnitude for an incident angle of θ=30° is shown in Fig. 7(a), along with the propagation direction indicated schematically by the white arrows. Note the bright standing wave pattern above the grid line and outside the structure, showing that light trapping is largely absent. To highlight the importance of light trapping we compare the performance of triangular wires with a flat-wire electrode. Note that a commonly used dome-shaped wire would outperform a flat electrode due to some degree of forward scattering by the inclined wire sides [37,41,42]. The case of intermediate surface angle (middle panel in Fig. 6(b)) is identical to a previously shown result (top panel in Fig. 4(b)), revealing the previously discussed onset of partial light trapping for an incident angle of 18°. The lower panel shows the light trapping efficiency for a large electrode surface tilt angle of α_s=30°. In this case the near-normal incidence results show ~85% light trapping efficiency even with this low cover layer index. This value is lower than the prediction from the ray optics model

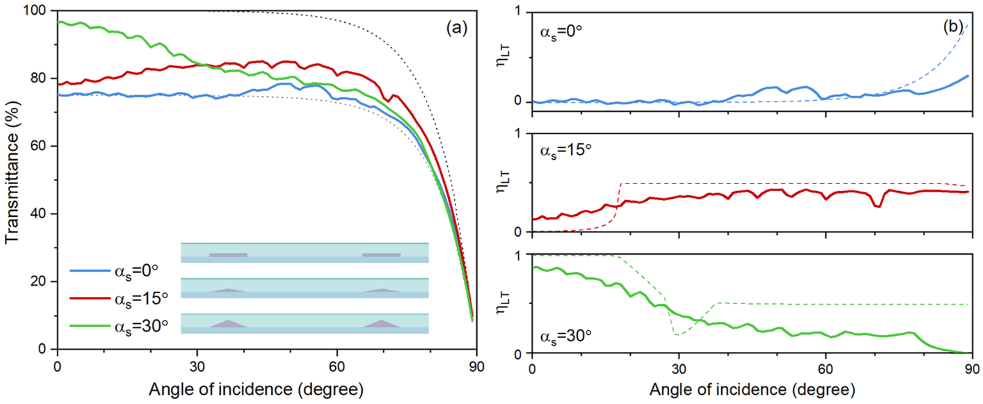

Fig. 6. (a) Transmittance of light trapping electrodes with f=0.25, W=2 µm, n_c=1.5, and D=1 µm for surface tilt angles α_s=0° (blue), 15° (red) and 30° (green). (b) Corresponding light trapping efficiencies from numerical calculations (solid lines) and ray optics (dashed lines).

(nearly 100%) because of diffractive effects, causing some of the reflected light to propagate at an angle below the critical angle. At an external angle of 18° the ray optics model predicts the onset of secondary shadowing, followed by loss of TIR at 28° and recovery of secondary shadowing as some of the reflected light passes over the next grid line. These effects cannot be clearly distinguished in the simulated data due to diffractive effects. The TE field magnitude distribution for normal incidence illumination is shown in Fig. 7(b). Note that zero reflection loss would produce a homogeneous field magnitude above the cover layer. The fact that a faint standing wave pattern is visible indicates the presence of some reflection loss due to a combination of diffractive effects and interactions with adjacent grid lines. Despite this small reflection loss, a total normal incidence transmission of 96% is achieved at 25% metal areal coverage.

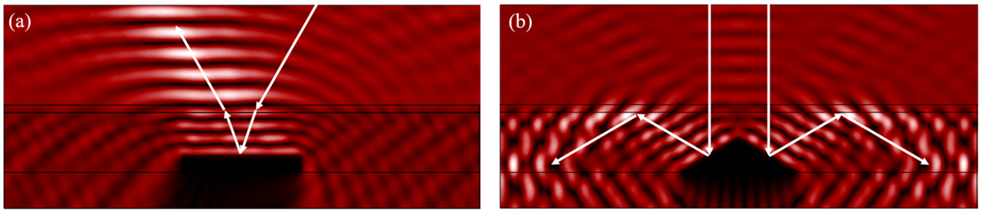

Fig. 7. TE field magnitude distributions for λ_0=600 nm, f=0.25, W=2 µm, D=1 µm and n_c=1.5 for surface tilt angles of (a) α_s=0° at 30° angle of incidence and (b) a surface tilt of α_s=30° at normal incidence.

6. Discussion and outlook

Figure 8 summarizes the main identified contributions to non-ideal optical transmission in interdigitated light trapping electrodes. First, any light incident at high angle will experience some top surface reflection loss (dashed cyan ray) even in the presence of an AR coating. This type of loss is also incurred in e.g. commercial encapsulated silicon solar cells. Second, for off-normal illumination, internally reflected light may propagate at an angle below the critical angle, resulting in a loss of TIR (dark blue ray). Finally, at large incident angle and small wire spacing, internally reflected light may impinge on an adjacent electrode, potentially leading to dissipation or escape from the light trapping structure (light blue ray). These effects can be mitigated by using a large cover layer index, a large surface tilt, a large wire spacing, and small cover layer thickness.

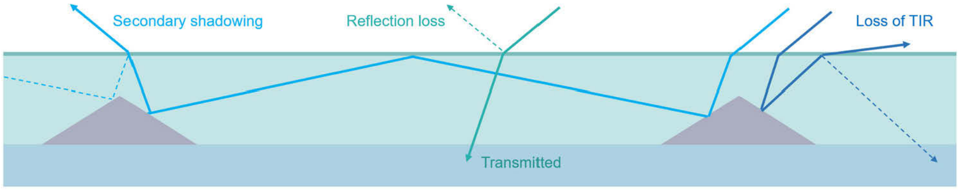

Fig. 8. Key optical loss mechanisms total transmission and light trapping efficiency. Dashed lines indicate relatively weak contributions. The cover layer and substrate are assumed to be index matched in this schematic.

Given the challenges discussed above, it is of interest to evaluate the complete spectrally dependent performance of a system that more closely resembles a real world device, for example an encapsulated silicon solar cell. Unlike the assumptions in the preceding discussions, here we consider a realistic index mismatch between the cover layer and the substrate. To represent a typical Si solar cell, we assume a glass cover layer [43] which has an index similar to typical encapsulation materials. The substate is represented by lossless but dispersive silicon. An ARC consisting of MgF_2 [44] with a thickness of 109 nm is used at the top surface, and an AlN [45] ARC is placed at the glass-silicon interface (62.5 nm thickness, n=2.2). The cover layer thickness is set to D=1.1 µm, the metal coverage is set to f=0.1 with an electrode width W=2 µm and a surface angle of α_s=30°.

Figure 9(a) shows a schematic of a single grid line in the simulated structure. Figure 9(b) shows the angle dependent reflection spectrum for this structure at f=0.1. The large reflection losses at short wavelength are largely due to top surface reflection, due to the non-ideal AR response of the thin MgF_2 layer at short wavelengths. Figure 9(c) shows the corresponding light trapping efficiency spectra. Note that at angles up to 30° shadowing losses are reduced by more than a factor two for all wavelengths (colors yellow through green). The spectrally averaged shadowing reduction over a wide angular range (−60° to 60°) under AM1.5 solar irradiation [46] is 56.1%. The simulated structure shows a nearly polarization-independent spectrally averaged optical transmission of T=90.2% (T_{TE}=89.8% and T_{TM}=90.7%). These results demonstrate that even in a challenging real-world situation with large index mismatch between substrate and cover layer, shadowing losses can be reduced by more than a factor two over a wide angular and spectral range using compact light trapping electrodes. The effective sheet resistance of this structure is R_{sh}=0.22 Ω/sq., far below typical industrial requirements (R_{sh}<100 Ω/sq.) [34,35], demonstrating the unique possibility of simultaneously achieving low shadowing losses and high electrical conductivity.

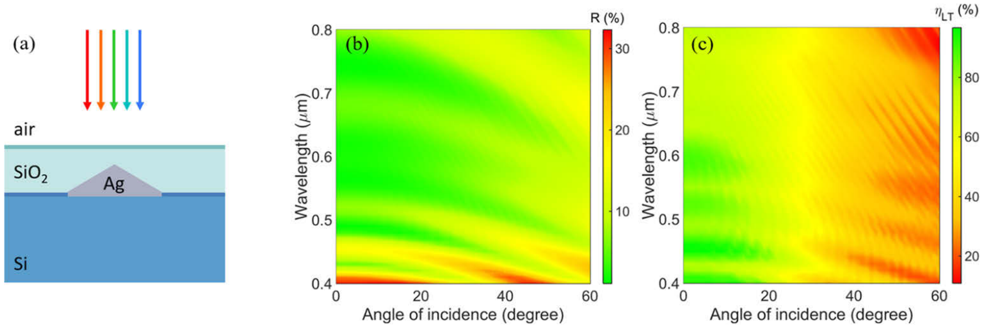

Fig. 9. (a) Schematic of a light trapping transparent silver electrode on an encapsulated silicon solar cell. (b) Reflectance and (c) light trapping efficiency of an encapsulated Si solar cell with f=0.1, W=2 µm, D=1.1 µm and α_s=30°.

7. Summary

The angle dependent optical response of triangular light trapping electrodes was investigated numerically and analytically. A ray optics model was developed to predict the transmission of light trapping electrodes. Three effects that adversely affect light trapping were identified: partial loss of TIR at large angle of incidence and the absorptive and radiative loss due interaction with the neighboring electrodes (secondary shadowing). Additionally, the light trapping performance was evaluated in terms of the light trapping efficiency that represents the reduction of shadowing losses. The influences of surface tilt angle, cover layer thickness and cover layer index on the light trapping efficiency were investigated. Electrodes with higher cover layer index, larger tilt angle and smaller cover layer thickness were found to enable high light trapping efficiency. Using realistic materials it was found that shadowing losses in a silicon solar cell with 10% metal coverage and an effective sheet resistance of 0.22 Ω/sq can be reduced by 56% averaged over a 120° angular range and spectrally averaged over the AM1.5 solar spectrum.

Funding. National Science Foundation (ECCS-1650002).

Disclosures. The authors declare no conflicts of interest.

Data availability. Data underlying the results presented in this paper are not publicly available at this time but may be obtained from the authors upon reasonable request.

References

1. T. Sannicolo, M. Lagrange, A. Cabos, C. Celle, J. P. Simonato, and D. Bellet, "Metallic Nanowire-Based Transparent Electrodes for Next Generation Flexible Devices: a Review," Small **12**(44), 6052–6075 (2016).
2. Z. Liu, J. Xu, D. Chen, and G. Shen, "Flexible electronics based on inorganic nanowires," Chem. Soc. Rev. **44**(1), 161–192 (2015).
3. P. Kou, L. Yang, C. Chang, and S. He, "Improved Flexible Transparent Conductive Electrodes based on Silver Nanowire Networks by a Simple Sunlight Illumination Approach," Sci Rep **7**(1), 42052 (2017).
4. K. Ellmer, "Past achievements and future challenges in the development of optically transparent electrodes," Nat. Photonics **6**(12), 809–817 (2012).
5. S. J. Kim, J.-H. Kang, M. Mutlu, J. Park, W. Park, K. E. Goodson, R. Sinclair, S. Fan, P. G. Kik, and M. L. Brongersma, "Anti-Hermitian photodetector facilitating efficient subwavelength photon sorting," Nat. Commun. **9**(1), 316 (2018).
6. E. C. Garnett, W. Cai, J. J. Cha, F. Mahmood, S. T. Connor, M. Greyson Christoforo, Y. Cui, M. D. McGehee, and M. L. Brongersma, "Self-limited plasmonic welding of silver nanowire junctions," Nat Mater **11**(3), 241–249 (2012).
7. V. E. Ferry, J. N. Munday, and H. A. Atwater, "Design Considerations for Plasmonic Photovoltaics," Adv. Mater. **22**(43), 4794–4808 (2010).
8. J. van de Groep, P. Spinelli, and A. Polman, "Transparent conducting silver nanowire networks," Nano Lett. **12**(6), 3138–3144 (2012).
9. V. E. Ferry, L. A. Sweatlock, D. Pacifici, and H. A. Atwater, "Plasmonic Nanostructure Design for Efficient Light Coupling into Solar Cells," Nano Lett. **8**(12), 4391–4397 (2008).
10. L. Hu, H. S. Kim, J.-Y. Lee, P. Peumans, and Y. Cui, "Scalable Coating and Properties of Transparent, Flexible, Silver Nanowire Electrodes," ACS Nano **4**(5), 2955–2963 (2010).
11. H. A. Atwater and A. Polman, "Plasmonics for improved photovoltaic devices," Nat. Mater. **9**(3), 205–213 (2010).
12. V. E. Ferry, M. A. Verschuuren, H. B. T. Li, E. Verhagen, R. J. Walters, R. E. I. Schropp, H. A. Atwater, and A. Polman, "Light trapping in ultrathin plasmonic solar cells," Opt. Express **18**(S2), A237–A245 (2010).
13. R. Saive and H. A. Atwater, "Mesoscale trumps nanoscale: metallic mesoscale contact morphology for improved light trapping, optical absorption and grid conductance in silicon solar cells," Opt. Express **26**(6), A275–A282 (2018).
14. H.-P. Wang and J.-H. He, "Toward Highly Efficient Nanostructured Solar Cells Using Concurrent Electrical and Optical Design," Adv. Energy Mater. **7**(23), 1602385 (2017).
15. X. Wang, L. Zhi, and K. Müllen, "Transparent, Conductive Graphene Electrodes for Dye-Sensitized Solar Cells," Nano Lett. **8**(1), 323–327 (2008).
16. Z. Wu, "Transparent, Conductive Carbon Nanotube Films," Science **305**(5688), 1273–1276 (2004).
17. H. Lu, X. Ren, D. Ouyang, and W. C. H. Choy, "Emerging Novel Metal Electrodes for Photovoltaic Applications," Small **14**(14), 1703140 (2018).
18. J.-Y. Lee, S. T. Connor, Y. Cui, and P. Peumans, "Solution-Processed Metal Nanowire Mesh Transparent Electrodes," Nano Lett. **8**(2), 689–692 (2008).
19. D. S. Ghosh, T. L. Chen, and V. Pruneri, "High figure-of-merit ultrathin metal transparent electrodes incorporating a conductive grid," Appl. Phys. Lett. **96**(4), 041109 (2010).
20. P. Kuang, J. M. Park, G. Liu, Z. Ye, W. Leung, S. Chaudhary, D. Lynch, K. M. Ho, and K. Constant, "Metal-nanowall grating transparent electrodes: achieving high optical transmittance at high incident angles with minimal diffraction," Opt. Express **21**(2), 2393–2401 (2013).
21. S. Ye, A. R. Rathmell, Z. Chen, I. E. Stewart, and B. J. Wiley, "Metal nanowire networks: the next generation of transparent conductors," Adv. Mater. **26**(39), 6670–6687 (2014).
22. S. De, T. M. Higgins, P. E. Lyons, E. M. Doherty, P. N. Nirmalraj, W. J. Blau, J. J. Boland, and J. N. Coleman, "Silver Nanowire Networks as Flexible, Transparent, Conducting Films: Extremely High DC to Optical Conductivity Ratios," ACS Nano **3**(7), 1767–1774 (2009).
23. A. W. Blakers, "Shading losses of solar-cell metal grids," J. Appl. Phys. **71**(10), 5237–5241 (1992).
24. F. H. Chen, S. Pathreeker, J. Kaur, and I. D. Hosein, "Increasing light capture in silicon solar cells with encapsulants incorporating air prisms to reduce metallic contact losses," Opt. Express **24**(22), A1419–A1430 (2016).
25. J. N. Munday and H. A. Atwater, "Large Integrated Absorption Enhancement in Plasmonic Solar Cells by Combining Metallic Gratings and Antireflection Coatings," Nano Lett. **11**(6), 2195–2201 (2011).
26. R. B. Stephens and G. D. Cody, "Optical reflectance and transmission of a textured surface," Thin Solid Films **45**(1), 19–29 (1977).
27. W. H. Southwell, "Pyramid-array surface-relief structures producing antireflection index matching on optical surfaces," J. Opt. Soc. Am. A **8**(3), 549–553 (1991).
28. J. A. Dobrowolski, D. Poitras, P. Ma, H. Vakil, and M. Acree, "Toward perfect antireflection coatings: numerical investigation," Appl. Opt. **41**(16), 3075–3083 (2002).

29. X. Yan, D. J. Poxson, J. Cho, R. E. Welser, A. K. Sood, J. K. Kim, and E. F. Schubert, "Enhanced Omnidirectional Photovoltaic Performance of Solar Cells Using Multiple-Discrete-Layer Tailored- and Low-Refractive Index Anti-Reflection Coatings," Adv. Funct. Mater. **23**(5), 583–590 (2013).
30. E. Parvazian, F. Karimzadeh, and M. H. Enayati, "Photovoltaic Characterization and Electrochemical Impedance Spectroscopy Analysis of Dye-Sensitized Solar CellsBased on Composite TiO2–MWCNT Photoelectrodes," J. Electron. Mater. **43**(5), 1450–1459 (2014).
31. D. Barettin, A. Di Carlo, R. De Angelis, M. Casalboni, and P. Prosposito, "Effect of dielectric Bragg grating nanostructuring on dye sensitized solar cells," Opt. Express **20**(S6), A888–A897 (2012).
32. R. Saive, T. C. R. Russell, and H. A. Atwater, "Light Trapping in Bifacial Solar Modules Using Effectively Transparent Contacts (ETCs)," in *2018 IEEE 7th World Conference on Photovoltaic Energy Conversion (WCPEC) (A Joint Conference of 45th IEEE PVSC, 28th PVSEC & 34th EU PVSEC)*, 2018), 0045–0048.
33. T. S. Liang, M. Pravettoni, C. Deline, J. S. Stein, R. Kopecek, J. P. Singh, W. Luo, Y. Wang, A. G. Aberle, and Y. S. Khoo, "A review of crystalline silicon bifacial photovoltaic performance characterisation and simulation," Energy Environ. Sci. **12**(1), 116–148 (2019).
34. R. Zhang and M. Engholm, "Recent Progress on the Fabrication and Properties of Silver Nanowire-Based Transparent Electrodes," Nanomaterials **8**(8), 628 (2018).
35. H.-C. Chu, Y.-C. Chang, Y. Lin, S.-H. Chang, W.-C. Chang, G.-A. Li, and H.-Y. Tuan, "Spray-Deposited Large-Area Copper Nanowire Transparent Conductive Electrodes and Their Uses for Touch Screen Applications," ACS Appl. Mater. Interfaces **8**(20), 13009–13017 (2016).
36. P. G. Kik, "Catoptric electrodes: transparent metal electrodes using shaped surfaces," Opt. Lett. **39**(17), 5114–5117 (2014).
37. M. Sun and P. G. Kik, "Scale dependent performance of metallic light-trapping transparent electrodes," Opt. Express **28**(12), 18112–18121 (2020).
38. P. B. Johnson and R. W. Christy, "Optical Constants of the Noble Metals," Phys. Rev. B **6**(12), 4370–4379 (1972).
39. CST Studio Suite, Dassault Systèmes Simulia, Providence, Rhode Island, 2017.
40. M. G. Moharam and T. K. Gaylord, "Rigorous coupled-wave analysis of planar-grating diffraction," J. Opt. Soc. Am. **71**(7), 811–818 (1981).
41. D. Li, X. Liu, X. Chen, W.-Y. Lai, and W. Huang, "A Simple Strategy towards Highly Conductive Silver-Nanowire Inks for Screen-Printed Flexible Transparent Conductive Films and Wearable Energy-Storage Devices," Adv. Mater. Technol. **4**(8), 1900196 (2019).
42. X. Xu, Z. Liu, P. He, and J. Yang, "Screen printed silver nanowire and graphene oxide hybrid transparent electrodes for long-term electrocardiography monitoring," J. Phys. D: Appl. Phys. **52**(45), 455401 (2019).
43. I. H. Malitson, "Interspecimen Comparison of the Refractive Index of Fused Silica," J. Opt. Soc. Am. **55**(10), 1205–1209 (1965).
44. M. J. Dodge, "Refractive properties of magnesium fluoride," Appl. Opt. **23**(12), 1980–1985 (1984).
45. J. Pastrňák and L. Roskovcová, "Refraction Index Measurements on AlN Single Crystals," Phys. Status Solidi B **14**(1), K5–K8 (1966).
46. ASTM Standard G173, *Standard Tables for Reference Solar Spectral Irradiances: Direct Normal and Hemispherical on 37° Tilted Surface, American Society for Testing and Materials*, West Conshocken, PA, USA.